A bioinspired approach to fabricate fluorescent nanotubes with strong water adhesion by soft template electropolymerization and post-grafting

Ananya Sathanikan, Giacomo Ceccone, Jorge Bañuls-Ciscar, Miaobo Pan, Fadwa Kamal, Talia Bsaibess, Anne Gaucher, Damien Prim, Rachel Méallet-Renault, Pascal Colpo, et al.

Graphical Abstract

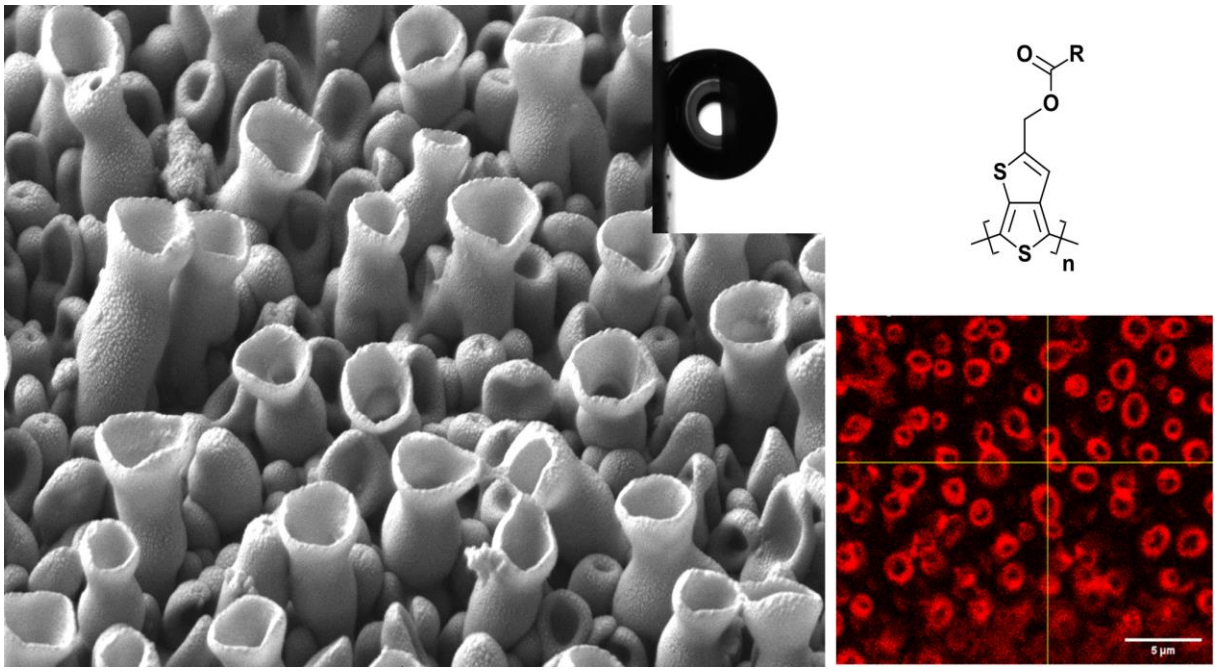

A bioinspired approach to fabricate fluorescent nanotubes with strong water adhesion by soft template electropolymerization and *post*-grafting

Ananya Sathanikan[a], Giacomo Ceccone[b], Jorge Bañuls-Ciscar[b], Miaobo Pan,[c] Fadwa Kamal[d], Talia Bsaibess[d], Anne Gaucher[d], Damien Prim[d], Rachel Méallet-Renault[c], Pascal Colpo[b], Sonia Amigoni[a], Frédéric Guittard[a], and Thierry Darmanin[a,*]

[a] *Université Côte d'Azur, NICE Lab, 06100 Nice, France.*

Corresponding author: thierry.darmanin@unice.fr ; Tel : +33 6 34 12 10 13.

[b] *European Commission, DG Joint Research Centre, TP125, Via Fermi, 21027 Ispra, Italy.*

[c] *University Paris-Saclay, Institut des Sciences Moléculaires d'Orsay (ISMO), CNRS, F-91405 Orsay, France*

[d] *Université de Versailles St-Quentin, UMR CNRS 8180, Institut Lavoisier de Versailles, 45, avenue des Etats-Unis, 78035 Versailles Cedex, France*

Abstract

Hypothesis

In this original work, we aim to control both the surface wetting and fluorescence properties of extremely ordered and porous conducting polymer nanotubes prepared by soft template electropolymerization and *post*-grafting. For reaching this aim, various substituents of different hydrophobicity and fluorescence were *post*-grafted and the post-grafting yields were evaluated by surface analyses. We show that the used polymer is already fluorescent before post-grafting while the post-grafting yield and as a consequence the surface hydrophobicity highly depends on the substituent.

Experiments

Here, we have chosen to chemically grafting various fluorinated and aromatic substituents using a *post*-grafting in order to keep the same surface topography. Flat conducting polymer surfaces with similar properties have been also prepared for determining the surface energy with the Owens-Wendt equation and estimating the *post*-grafting yield by X-ray Photoemission Spectroscopy (XPS) and Time of Flight Secondary Emission Spectrometry (ToF-SIMS). For example, using fluorinated chains of various length (C_4F_9, C_6F_{13} and C_8F_{17}), it is demonstrated that the surface hydrophobicity and oleophobicity do not increase with the fluorinated chain length due to the different *post*-grafting yields and because of the presence of nanoroughness after *post*-grafting.

Findings

These surfaces have high apparent water contact angle up to 130.5° but also strong water adhesion, comparable to rose petal effect even if there are no nanotubes on petal surface. XPS and ToF-SIMS analyses provided a detailed characterisation of the surface chemistry with a qualitative classification of the grafted surfaces (F6 > F4 > F8). SEM analysis shows that

grafting does not alter the surface morphology. Finally, fluorescence analyses show that the polymer surfaces before *post*-treatment are already nicely fluorescent. Although the main goal of this paper was and is to understand the role of surface chemistry in tailoring the wetting properties of these surfaces rather than provide specific application examples, we believe that the obtained results can help the development of specific nanostructured materials for potential applications in liquid transport, or in stimuli responsive antimicrobial surfaces.

Keywords: Surface functionalization, Wettability, Hydrophobicity, Surface analysis, Fluorescence, Conducting polymers, Nanotubes.

1. Introduction

The difficulty in obtaining regular nanoscale structures is a key challenge especially when we want to find a relationship between unique properties and the shape of these structures [1–6]. In Nature, nanostructures are omnipresent and for example allowing geckos to strongly adhere and walk to various surfaces [7–10]. In wettability field, the scientific communauty focus on vertically aligned nanotubes for their surface-area-to-volume ratio allowing to control the wetting properties with their dimensions (diameter, height, porosity, shape) [11–14]. Well-defined vertically aligned nanotubes are often prepared using membranes with the defined features. One of the most used membrane is anodized aluminium oxide (AAO) membrane [15–17]. However, one membrane is necessary for each nanotube dimension.

Alternatively, the nanotube dimensions and even the shape can be easily and fastly tuned by templateless electropolymerization, which is a soft template electropolymerization. Gas bubbles play the role of soft template while the polymer electrodeposited around these bubbles. In the literature, the soft template electropolymerization of pyrrole in water (H_2O) has been specifically studied [18–23]. During electropolymerization, H_2O can be oxidized and/or reduced to form H_2/O_2 bubbles following the chosen electropolymerization method (potentiostatic [18,19] or potentiodynamic methods [20–23]). However, this method needs water-soluble monomer such as pyrrole while a surfactant is often necessary to stabilize the gas bubbles.

Given the low water solubility of most of the monomers r, this process was also tested in organic solvent (e. g. dichloromethane) and works as soon as trace H_2O is present in solution.

It is even possible to replace surfactant using rigid monomers highly favouring π-stacking interactions [24–27]. Moreover, very recently it was even clearly demonstrated the presence of reverse micelles stabilized by the monomer and the electrolyte before electropolymerization [28]. Although in these works low H_2O content was used, it was demonstrated that sometimes it is preferable to saturate CH_2Cl_2 with H_2O in order to form a large number of nanotubes [28].

However, for studying the influence of surface energy on nanotubular structures by electropolymerization, it is preferable to *post*-graft the substituents because they have a huge influence on the surface structures [29]. In this original work, vertically aligned open nanotubes with functional hydroxyl groups have been prepared by templateless electropolymerization of thieno[3,4-*b*]thiophen-2-ylmethanol (**Thieno-OH**) in CH_2Cl_2 saturated with H_2O (CH_2Cl_2 + H_2O) in order to release a very high amount of gas bubbles, to form densely packed nanotubes and with just with one deposition scan in order to keep the nanotubes open. Indeed, we already demonstrated with NaphDOT [28] that if the polymer is intrinsically hydrophilic (Young's angle of PolyNaphDOT θ^Y_w = 63.6°), if we want to highly increase the water contact angle (θ_w), it is preferable to form densely packed open nanotubes with a nanometric size (height and diameter). In this work, the formation of densely packed nanotubes was performed by using the solvent CH_2Cl_2 + H_2O while the formation of open tubes was done by choosing the cyclic voltammetry as the electropolymerization process because a much higher of gas bubbles is released with this process compared to deposition at constant potential, for example. Then, the nanometric size of the nanotubes was possible by using just one deposition scan.

Then, various substituents have been *post*-grafted for changing both the surface wettability and fluorescent properties by simple esterification reaction (Scheme 1). If the surface *post*-grafting was already in the literature with different chemical reactions [30,31], here, to our knowledge, this is the first time we have tried to better explain the wettability results of rough surfaces by determining the post-grafting yields with each substituent. The main of this paper is to underline and to understand the role of surface chemistry in tailoring the wetting properties of these rough surfaces.

The influence of the surface tubular structures on the wettability properties has been possible by preparing smooth surfaces with **Thieno-OH** and *post*-grafted with each substituent. Hence, with these smooth surfaces, their surface energy has been determined with the Owens-Wendt

reaction with three liquid probes while the *post*-grafting yield with each substituent could be estimated by XPS and ToF-SIMS analyses.

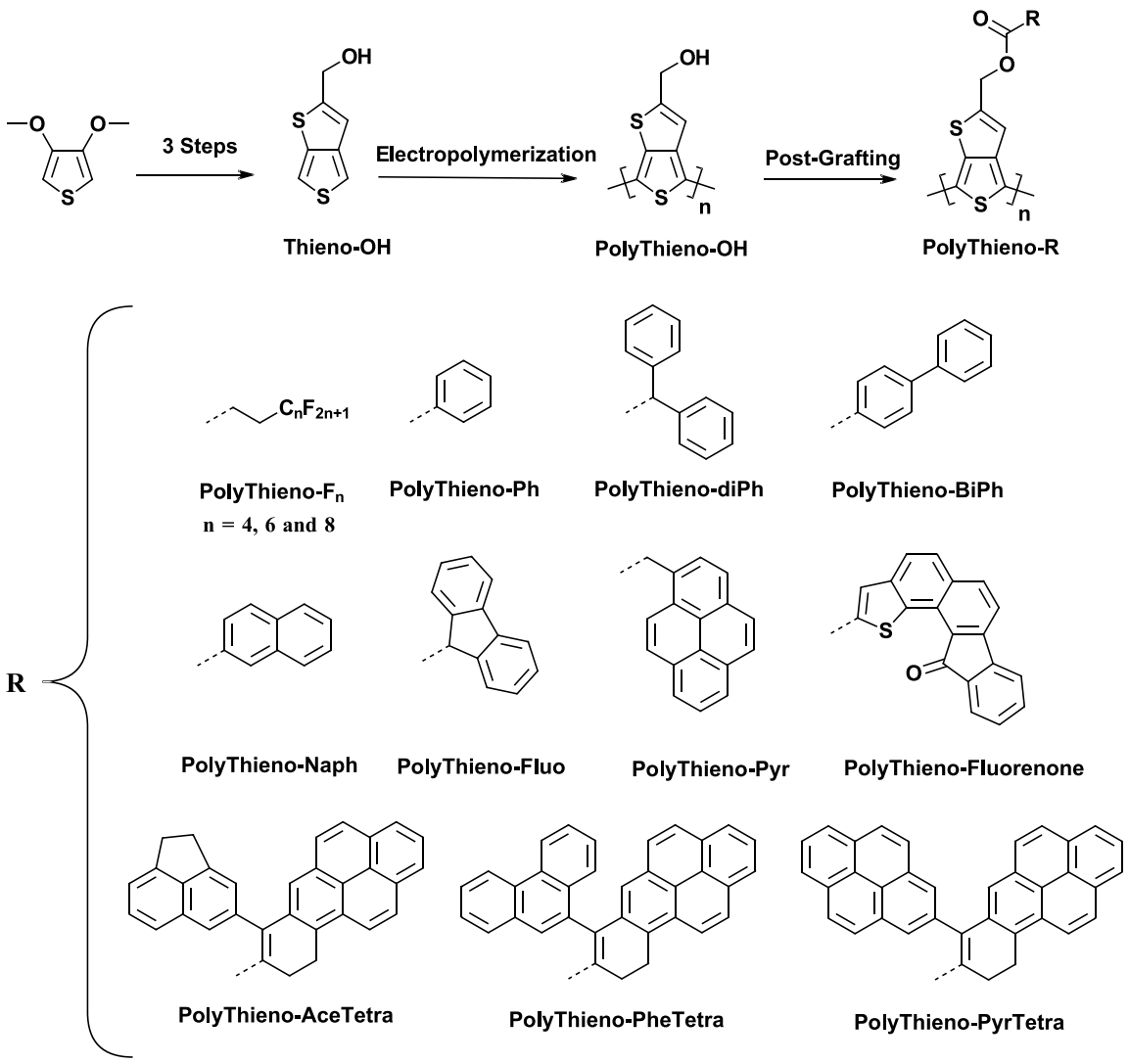

Scheme 1. Strategy used to form conducting polymer nanotubes with various substituents.

2. Materials and methods

2.1. Formation of nanotubes by soft template electropolymerization

Thieno[3,4-*b*]thiophen-2-ylmethanol (**Thieno-OH**) was synthesized according to a previous work [29]. In order to perform a huge number of nanotubes, CH_2Cl_2 was saturated with H_2O (CH_2Cl_2 + H_2O). This solvent was prepared by simply mixing CH_2Cl_2 and H_2O and keeping the organic phase after decantation. 0.1 M of tetrabutylammonium perchlote (Bu_4NClO_4) as supporting electrolyte and 0.01 M of **Thieno-OH** as the monomer were added to CH_2Cl_2 + H_2O. For the depositions, a potentiostat (Autolab from Metrohm) *via* three electrode system was used. The electrodes consisted in 2 cm^2 Indium Tin Oxide (ITO)-coated glass as the working electrode, a glassy carbon rod as the counter-electrode and a saturated calomel

electrode (SCE) as the reference electrode. Here, ITO was selected especially for the fluorescence tests. Here, the depositions were performed by cyclic voltammetry in order to release a high amount a gas necessary to form porous structures (nanotubes) and with just with 1 deposition scan in order to keep the nanotubes open. More precisely, the formation of nanotubes was obtained by doing 1 deposition scan from -1 V to the monomer oxidation potential (E^{ox} = 1.77 V *vs* SCE) at the scan rate of 20 mV s^{-1}.

2.2. Formation of smooth surfaces by electropolymerization

For the formation of smooth surfaces, CH_2Cl_2 was used as the solvent. Here, in order to form smooth surfaces, the depositions were performed at constant potential (E^{ox} = 1.77 V *vs* SCE) and using an ultra-short deposition charge of 1 mC cm^{-2}. However, in order to have the same polymer that by cyclic voltammetry that means in its reduced state, the polymer was reduced by cyclic voltammetry but just 1 back scan from E^{ox} = 1.77 V to -1 V at the scan rate of 20 mV s^{-1}.

2.3. *Post*-grating

The synthesis of the molecules for *post*-grafting is available in Supporting Information. A glass flask containing 20 mL of CH_2Cl_2 and a large excess of dicyclohexylcarbodiimide (DCC) (80 mg) and the corresponding acid (80 mg), and a catalytic amount 4-dimethylaminopyridine (DMAP) is stirred for 30 mn. Then, the coated-substrates were added and the flask is slightly stirred for 5 days. Finally, the substrates were washed with CH_2Cl_2 and slowly dried.

2.4. Surface characterization

After metallization, surfaces nanostructures were imaged *via* scanning electron microscopy (SEM) (6700F microscope from JEOL) with and without surface incination of 45° in order to better estimate the height of the nanotubes. The surface wettability was characterized *via* goniometer (DSA30 from Bruker) by placing water droplets on the substrate and measuring the apparent contact angles with water (θ_w) taken at the triple point (n=5). For the contact angle hysteresis and sliding angles, the substrate was inclined until the droplets moved, using a procedure described by Amirfazli [32]. The advanced and receding contact angles are taken in leading edge and trailing edge, respectively, of the droplets just before their moving due to

gravity. If the droplets do not move even if the sliding angle is above 90°, the substrate is highly adhesive and parahydrophobic, as described by Marmur [6].

2.5. Surface analysis: XPS and ToF-SIMS

The surface chemistry after functionalization was assessed by X-Ray Photoemission Spectroscopy (XPS) and Time of Flight Secondary Ion Mass Spectrometry (ToF-SIMS).

Samples were cleaned in hexane and then mounted on sample holder using a silicon free, UHV compatible double side Cu tape (3M, USA). The samples were then inserted in a load-lock for overnight degassing ($p = 5x10^{-8}$ mbar) and finally in the analysis chamber (base pressure $5x10^{-9}$ mbar). XPS analysis was carried out by means of a Axis Ultra-DLD spectrometer (Kratos Analytical, UK) equipped with a monochromatic Al Kα source ($h\nu$ = 1486.6 eV) operating at 150W. Wide scan spectra were recorded from 0 to 1100 eV binding energy in hybrid mode, "slot" (400 x 700 μm^2 analysis area) and FoV2 (100 μm spot) at 80eV and 160 eV pass energy, whereas core level spectra were recorded in "hybrid" mode using pass energy of 20 eV. The take-off angle (ToA) respect to the sample normal was 0° for survey and high-resolution (HR) spectra, whilst angle-resolved XPS analyses (AR-XPS) were performed at ToA = 30°, 45° and 70°. Operating pressure was 1.5×10^{-8} mbar. Surface charging was compensated using low energy (~4 eV) electrons and adjusted using the charge balance plate on the instrument. Three different spots were analyzed for each sample. All the spectra were processed with CasaXPS (ver. 2.3.22). Spectra were calibrated setting hydrocarbon C1s at 285.0 eV. The surface composition was evaluated from the survey spectra, after background subtraction, using relative the sensitivity factors provided by the manufacturer. Peak fitting was performed with no preliminary smoothing. Lorentzian finite functions, LF(a,b,w,n), were used to approximate the line shapes of the fitting components after a Tougaard U3-type background subtraction [32,33].

ToF-SIMS (ToF IV, IONTOF GmbH, Germany) was also employed to characterize samples' chemistry. The accelerating voltage of the liquid metal ion gun (LMIG) was 25 keV, Bi_3^+ was employed as source of primary ions rastering over an area of 200 x 200 μm^2. The analyses were performed in static conditions keeping the ion dose below 10^{12} ions/cm^2. Acquisition time was 45 s, with a beam current of 0.5 pA and primary ion beam in pulsed mode. Negative mass spectra were collected while using an electron flood gun to dissipate surface charging. C^-, CH^-, CH_2^-, C_2H^-, C_3H^-, C_4H^- and C_5H^- peaks were used to calibrate the positive spectra and a peak-list was created using the SurfaceLab software (ver. 6, IONTOF GmbH). Given the large number of peaks and spectra, Multivariate Analysis (MVA) methods were used to aid in the interpretation of the data. MVA methods are widely used within the ToF-SIMS community and are designed to reduce the size of large data sets with a minimal loss of information [34–37]. Normalized intensities of all the peaks selected

in the peak-list were loaded into the SimsMVA software [38] where Non-negative Matrix Factorialization (NMF) and Principal Component Analyses (PCA) were performed, providing endmembers in the case of NMF and principal components in the case of PCA [39]. Scores and loadings are the typical outcome of PCA and NMF analysis. The scores describe the relationship between samples for each principal component/endmember, whereas the loadings provide information regarding how the variables (peak intensities) relate to each principal component/endmember [35–40].

2.6. Fluorescence microscopy on films

Fluorescence images were acquired using Leica TCS SP5-AOBS confocal laser scanning microscope. The surfaces were submerged in distilled water, and imaged using × 63- 1.4 numerical aperture plan apochromat oil immersion objective. The size of the *xy* image was 512 × 512 pixels (image sizes: 49.21 × 49.21 µm² and 24.60 × 24.60 µm²) recorded on 12 bits. Films were excited at 476 nm or 488 nm and the emission was collected from 500 to 640 nm or 520-700nm. Laser power was usually set around 30% and gain was adjusted in order to get signal. Each image corresponds to an average of 3 frames.

3. Results and discussion

3.1. Formation of nanotubes by soft template electropolymerization and *post*-grafting

Thieno-OH was used as monomer for the soft template electropolymerization process, and Bu_4NClO_4 as the electrolyte and dichloromethane (CH_2Cl_2) as solvent. In order to release a high amount of gas bubbles and as a consequence to obtain vertically aligned nanotubes, CH_2Cl_2 was saturated with water (H_2O). The solvent is called here CH_2Cl_2 + H_2O. The deposition was performed on ITO substrate by cyclic voltammetry from -1 V to the monomer oxidation potential (E^{ox} = 1.77 V *vs* SCE) because it allows releasing both O_2 and H_2 bubbles. Only 1 scan at a scan rate of 20 mV s^{-1} was selected as optimal parameter to obtain a high number of open nanotubes. The resulting surfaces was characterized by SEM (Figure 1). The pictures display the presence of huge open nanotubes with a diameter of roughly 1 µm and a height of 3 µm. Moreover, the presence of close nanotubes of lower size is also observed. It should also be noticed that the surface of the tubes is smooth. Then, the surfaces were *post*-treated with different acids by a simple esterification reaction in order to modify the surface properties. By *post*-treatment of a modified surface, it is expected that only a part of the reactive groups would be modified. This point will be discussed in next paragraph.

Representative SEM pictures after *post*-treatment with Fluorenone are presented in Figure 2. As expected, surface morphology is maintained but the presence of nano-roughness on the nanotube surfaces is observed.

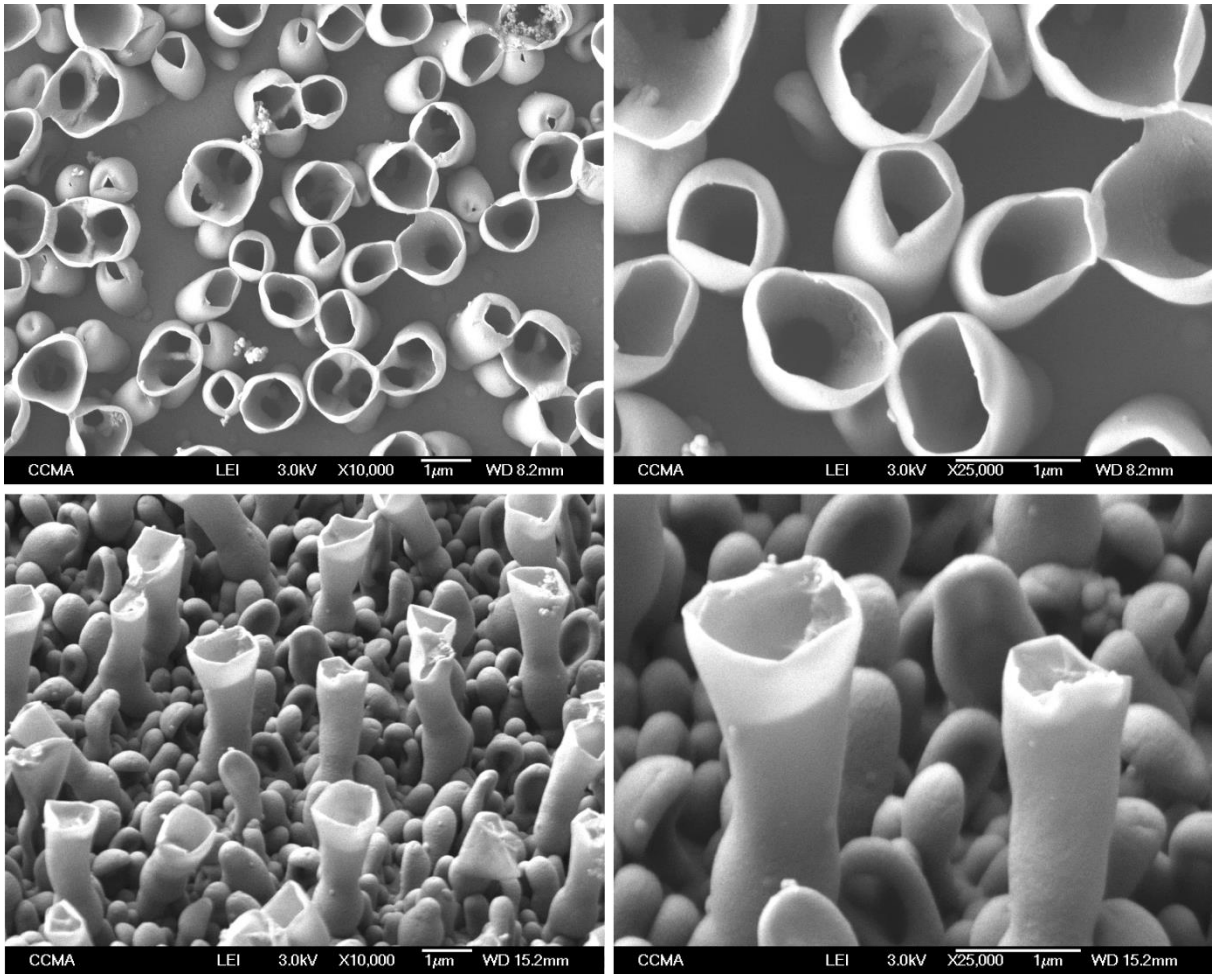

Figure 1. SEM images of the polymer surfaces electrodeposited from the monomer Thieno-OH (10 mM) in 0.1 M Bu_4NClO_4 / CH_2Cl_2 + H_2O in potentiodynamic conditions by cyclic voltammetry (E = –1 / +1.77 V) after 1 scan. The pictures are taken without (up) and with a substrate inclination of 45 ° (down).

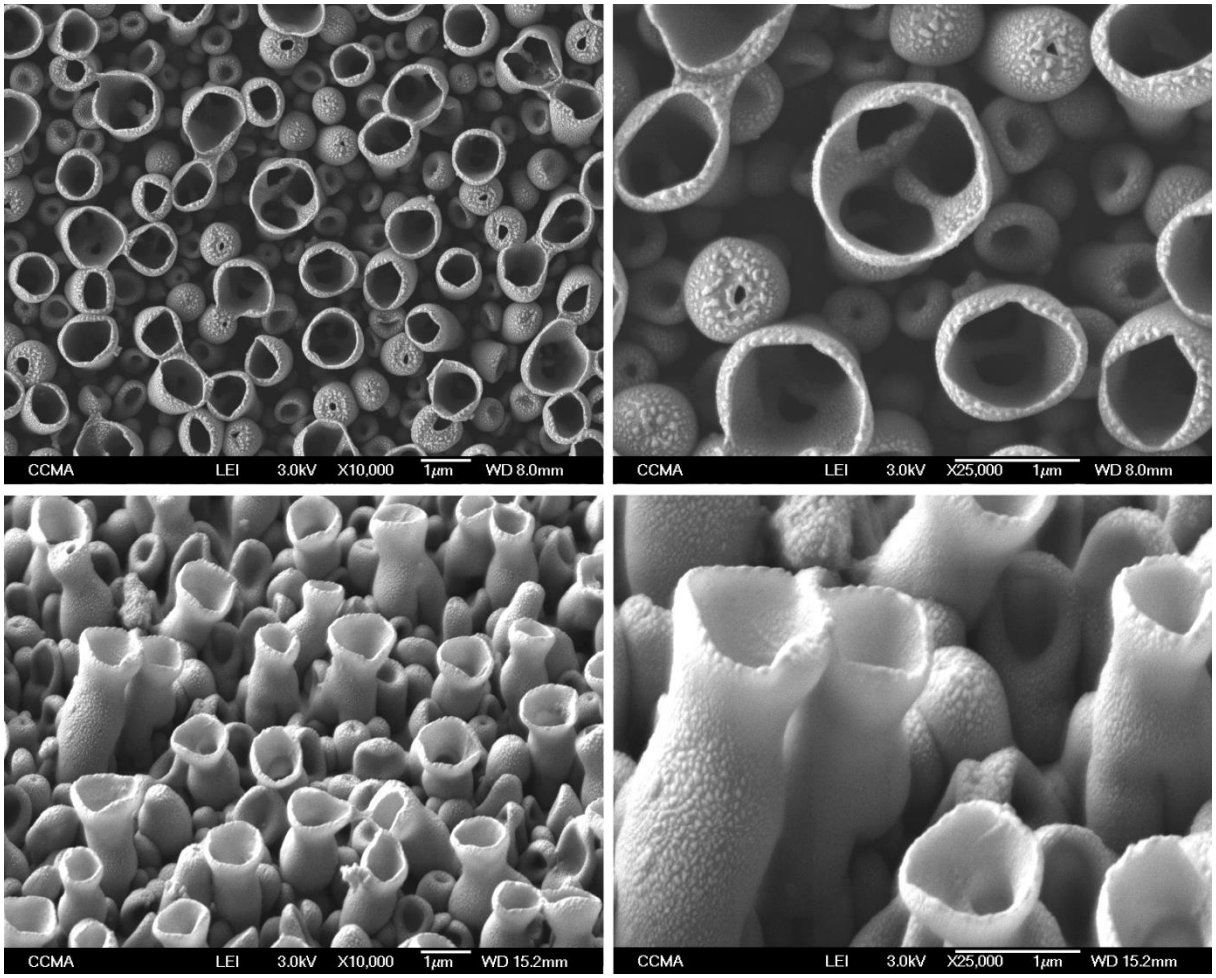

Figure 2. Representative SEM images of the polymer surfaces after *post*-treatment with fluorenone (PolyThieno-Fluorenone). The pictures are taken without (up) and with a substrate inclination of 45 ° (down).

3.2. Wetting properties

The apparent contact angles (θ) of the different surfaces are reported in Table 1. Surprisingly, even if the polymer has polar hydroxyl groups, PolyThieno-OH is slightly hydrophobic with a water contact angle of θ_{water} = 92.1°, indicating that the surface structures/roughness have an effect on contact angle. After *post*-treatment, the surfaces modified with fluorinated PolyThieno-F_8 have the highest hydrophobicity (θ_{water} up to 130.5°) and oleophobicity characters but these properties do not increase with the fluorinated chains lenght. Moreover, in order to have more information about the water adhesion of these substrates, we tried to determine the advancing (θ_{adv}) and receding (θ_{rec}) contact angles and as a consequence the contact angle hysteresis H = θ_{adv} - θ_{rec}. First, we tested the sessile drop method [41], that means by increasing and reducing the droplet volume but unfortunately it was not possible to determine the θ_{rec} because, due to the strong water adhesion, the triple-point line did not move

when the was sucked off. Then, the tilted-drop method was also tested [32], even if Krasovitski and Marmur demonstrated that the measured angles with this method did not exactly corresponded to θ_{adv} and θ_{rec} [42,43]. As shown in Figure 3, water droplets on these surfaces remained stuck even if the surfaces are inclined at 90° indication also of strong water adhesion but is was not possible to determine the θ_{adv} and the θ_{rec}. The strong adhesion of these surfaces in comparable to rose petals or gecko foot [8-10, 44-46]. Moreover, we tested water droplets from 1 µL to 50 µL and observed the sliding of the droplets only for droplets above 25 µL. These surfaces could be applied in the future in water harvesting systems because with these surfaces it is possible to collect small water droplet due to the high water adhesion while it would be possible to release the water droplet when their size increases [47].

In order to determine if the water droplet on these surfaces are in Wenzel state [48], Cassie-Baxter state [49] or intermediate states between the Wenzel and Cassie-Baxter, it was first necessary to determine the Young's angle [50] of these surfaces, that means the same surfaces but smooth. However, the droplets are not in the Cassie-Baxter state because it is admitted that the contact angle hysteresis has to be ultra-low that means only for trully superhydrophobic surfaces (lotus effect). It is also important to notice that to explain the strong water adhesion of rose petals, Bhushan and Nosonovsky demonstrated that several wetting regimes can coexist with the Wenzel, Cassie, lotus and petal [45]. Here, we use the term "intermediate states between the Wenzel and Cassie-Baxter" because we do not know exactly in which regime we are.

The Young equation [50] being dependent on the surface energy γ_{SV}, it was first necessary to determine γ_{SV} of the starting polymer (PolyThieno-OH) and after each *post*-treatment. Moreover, since the Young equation is valid only for smooth surfaces, γ_{SV} can be determined also only on smooth surfaces using the Owens-Wendt equation [51]. For this, smooth surfaces were prepared as described in the experimental section. These surfaces revealed very interesting properties (Table 2). In particular, as expected, PolyThieno-OH is clearly the most hydrophilic (θ^{Y}_{water} = 49.4°) due to the presence of hydroxyl groups and has the highest γ_{SV} = 52.8 mN m^{-1}. As expected, the polymers modified with fluorinated chains are intrinsically hydrophobic (θ^{Y}_{water} > 90°) have the highest hydrophobic and oleophobic character but surprisingly the lowest γ_{SV} = 22.7 mN m^{-1} is obtained with PolyThieno-F_6 and not PolyThieno-F_8. These results will be explained below by different *post*-grafting yields. The

polymers modified with aromatic groups have γ_{SV} between PolyThieno-OH and PolyThieno-F_n. The highest γ_{SV} = 47.3 mN m^{-1} is obtained with PolyThieno-Ph and the lowest γ_{SV} = 38.0 mN m^{-1} is obtained with PolyThieno-Fluorenone, which has $\theta^{Y}_{water} \approx 90°$ if we take into account the standard deviation. Hence, because only the fluorinated polymers being intrinsically hydrophobic ($\theta^{Y}_{water} > 90°$), only these surfaces may be in the Wenzel state otherwise it would be observed an increase of the surface hydrophilicity. For the same reason, except with PolyThieno-PheTetra for which $\theta_{water} \approx \theta^{Y}_{water}$, all the other surfaces are really in intermediate state between the Wenzel and Cassie-Baxter state because it is observed an increase of θ_{water} whereas $\theta^{Y}_{water} < 90°$. This may be due because water wet only the external part of the nanotubes but not the inner part [25]. It is also surprising to observe that the *post*-treatment with aromatic groups can induce sometimes an increase and sometimes a decrease of θ compare with PolyThieno-OH.

Table 1. Apparent contact angles (θ) with different probe liquids of different nantubular surfaces.

Polymer	θ_{water} [deg]	θ_{diiodo} [deg]	θ_{hexa} [deg]
PolyThieno-OH	92.1 ± 7.1	0	0
PolyThieno-F_4	129.0 ± 4.6	117.0 ± 5.5	30.5 ± 6.8
PolyThieno-F_6	122.7 ± 4.6	130.8 ± 0.9	83.4 ± 2.1
PolyThieno-F_8	130.5 ± 3.8	125.0 ± 4.9	90.7 ± 3.5
PolyThieno-Ph	98.6 ± 5.5	0	0
PolyThieno-diPh	115.0 ± 5.4	0	0
PolyThieno-BiPh	112.6 ± 3.5	0	0
PolyThieno-Naph	92.2 ± 5.8	0	0
PolyThieno-Fluo	98.4 ± 6.0	0	0
PolyThieno-Pyr	92.4 ± 6.4	0	0
PolyThieno-Fluorenone	112.0 ± 2.4	0	0
PolyThieno-AceTetra	85.8 ± 4.9	0	0
PolyThieno-PheTetra	79.8 ± 6.6	0	0
PolyThieno-PyrTetra	106.2 ± 2.3	0	0

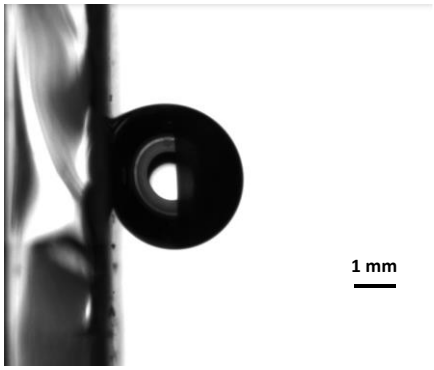

Figure 3. Picture of a water droplet on the polymer surfaces after *post*-treatment with F_6 (PolyThieno-F_6) with a substrate inclination of 90°.

Table 2. Apparent contact angles (θ) with different probe liquids as well as the surface energy of the corresponding smooth surfaces (γ_{sv}) and the dispersive (γ^D_{sv}) and polar (γ^P_{sv}) parts.

Polymer	θ^Y_{water} [deg]	θ^Y_{diiodo} [deg]	θ^Y_{hexa} [deg]	γ_{sv} [mN m^{-1}]	γ^D_{sv} [mN m^{-1}]	γ^P_{sv} [mN m^{-1}]
PolyThieno-OH	49.4 ± 3.0	36.8 ± 5.1	0	52.8	28.1	24.7
PolyThieno-F_4	95.3 ± 2.7	62.4 ± 1.5	33.1 ± 1.6	26.2	24.2	2.0
PolyThieno-F_6	101.4 ± 2.4	68.5 ± 2.1	42.8 ± 4.4	22.7	21.6	1.1
PolyThieno-F_8	100.4 ± 2.5	65.5 ± 1.5	35.7 ± 3.3	24.5	23.4	1.1
PolyThieno-Ph	61.6 ± 1.7	19.8 ± 4.8	0	47.3	32.6	14.7
PolyThieno-diPh	81.9 ± 2.8	20.5 ± 2.4	0	38.8	34.6	4.1
PolyThieno-BiPh	82.3 ± 2.6	17.8 ± 3.0	0	38.9	35.0	3.9
PolyThieno-Naph	78.2 ± 1.3	16.5 ± 2.9	0	40.2	34.7	5.5
PolyThieno-Fluo	69.5 ± 5.0	15.0 ± 3.9	0	43.7	33.9	9.8
PolyThieno-Pyr	78.5 ± 1.8	15.1 ± 5.5	0	40.3	34.9	5.4
PolyThieno-Fluorenone	90.7 ± 2.7	11.9 ± 1.9	0	38.0	36.7	1.3
PolyThieno-AceTetra	77.5 ± 0.4	12.9 ± 1.3	0	40.6	34.3	6.3
PolyThieno-PheTetra	76.9 ± 2.9	19.5 ± 5.0	0	39.8	35.0	4.8
PolyThieno-PyrTetra	79.9 ± 2.9	13.0 ± 2.6	0	40.3	36.7	1.3

3.3. Surface characterization by XPS and ToF-SIMS

In order to better understand these results, XPS and ToF-SIMS analyses were performed, especially for determining the *post*-grafting yield obtained with each substituent. Here, these techniques were chosen rather than infrared (IR) spectroscopy because ITO-coated glass absorbs IR.

In Table 3 the surface compositions of the samples are reported, whilst the correspondent survey spectra are illustrated in Figure S1. The theoretical compositions (excluding H) of the different compounds are reported in Table 4 and in Figure 4 the C1s core level spectra of the samples functionalized with the C_nF_{2n+1} SAMS are illustrated. As expected the intensities of the elements of ITO, namely In and Sn, together with the sulfur signal decrease in all samples after functionalization with all the molecules tested indicating a successful surface functionalization. The data related to the Indium Tin Oxide (ITO) substrate reveal the presence of a relatively high amount of carbon contamination routinely found on surfaces exposed to air (Figure 4a and Figure S2, supporting information), together with In, Sn and O peaks related to ITO. In particular, the C 1s spectrum can be fitted with three components corresponding to CC/CH (C1 285.00 eV, Figure 4a), C-O (C2 285.4 eV) and C=O, COOR (C3 288.9 eV). Analysis of In3d and Sn3d core level spectra reveals the presence of both In_2O_3 (In 3d 5/2 at 444.27 eV) and In-$(OH)_3$ (In 3d 5/2 at 445.08 eV, indicative of the presence of hydroxyl groups at the surface, whilst the Sn is present as SnO_2 (Sn 3d 5/2 at 486.7 eV), (Figure S2)) [52–54]. The O 1s core level spectrum of ITO can be fitted with three components corresponding to In_2O_3 (O1 at about 530 eV), SnO_2 and COOR (O2 at about 531.5 eV) and C-O/In$(OH)_3$ (O3 at about 532.3 eV) (Figure S2). After the functionalization with the Poly-Thieno-OH the surface composition changed drastically. A clear S 2p signal related to C-S appears at about 164 eV, whereas In and Sn concentrations decreased drastically. Moreover, C and O contents are also slightly reduced. The analysis of the S 2p core level reveals the presence of a of two separate doublets (Figure S3): the major doublet at 164.05 eV with a spin-orbit splitting of 1.16 eV is attributable to C-S bonds present in the Poly-Thieno compounds whilst the smaller doublet at 168 eV and spin orbit splitting of 1.25 eV is likely attributable to oxidized sulfur due to Thieno degradation during the reaction [55,56]. Finally, the C1s core level spectrum is largely different respect to that of ITO (Figure 4 b). It is noticed a slight shift (~ 0.3 eV to lower binding energies) and intensity increase of the component C2 (286.5 eV) related to the C-O bonds and the C3 (~ 288 eV, O-C=O/COOR), while two additional components C4 and C5, attributable to aromatic satellites are also observed [57]. The O 1s core level spectrum is also affected by the presence of the

Thione-OH molecules: as illustrated in fugure S3. In particular, the intensity component O1 is strongly reduced indicating the coverage of the ITO substrate, while the O2 is shifted toward higher binding energies because of the presence of C-O moieties; finally the O3 is also shifted toward higher binding energy and strongly reduced in intensities.

After functionalization with C_nF_{2n} compounds , the appearance of F 1s peak at about 688 eV (Figure S1) is a clear indication of the grafting of the hydrophobic molecules onto the ITO surface supporting the results of CA measurements (Table 1). Looking at the theoretical compositions of the functionalizing compounds presented in Table 4 one should expect an increase of F concentration when going from PolyThieno-F_4 to F_8 with a correspondent decreases of In, Sn and S signals. However, the F/C ratios are lower than the theoretical ones expected in case of full functionalization (Table 3 and 4). Furthermore, the fluorine concentration is lower in the case of PolyThieno-F_8 sample indicating a less degree of functionalization. This is supported by the higher content of indium, sulfur and oxygen compared to the PolyThieno-F_6 sample. These data are also supported by the analysis of the C 1s core level spectra illustrated in Figure 4. The functionalization with the Poly-Thieno-F_n is reflected in the appearance of the components at about 291 (CF_2) and 293 eV (CF_3), Figure 4 c-e. The ratios between these components are in agreement with the C_nF_{2n+1} theoretical compositions [58,59]. However, it is evident that the intensities of the C_n-F_{2n+1} component are as follows F6 > F4 > F8 supporting the conclusion of a different degree of grafting.

Table 3. Surface compositions obtained from XPS survey spectra.

	Concentration (at%)						
Sample ID	C1s	O1s	F1s	S2p	In3d	Sn3d	Rest Si, Ca,N, Cl
ITO	67.57 (4.51)	20.35 (2.04)	--	--	9.65 (2.43)	1.33 (0.17)	<2
PolyThieno-OH	61.43 (2.10)	17.91 (1.60)	--	13.73 (1.76)	4.23 (1.81)	0.50 (0.28)	<1
PolyThieno-F_4	47.43 (0.73)	20.03 (1.03)	20.17 (0.99)	6.26 (0.36)	4.22 (0.69)	0.82 (0.05)	<1

PolyThieno-F_6	48.64 (1.76)	14.28 (0.71)	28.58 (1.34)	6.28 (0.29)	0.71 (0.55)	0.37 (0.06)	<1
PolyThieno-F_8	55.44 (1.69)	18.76 (1.99)	15.59 (1.59)	7.47 (1.42)	1.42 (0.47)	0.37 (0.05)	<1
PolyThieno-Ph	66.27 (1.77)	23.14 (1.42)		7.70 (1.259	1.29 (0.17)	0.17 (0.02)	0.97 (0.40)
PolyThieno-diPh	78.64 (0.65)	11.77 (0.83)	--	7.94 (0.43)	0.69 (0.22))	0.07 (0.04)	0.6 (0.42)
PolyThieno-BiPh	71.22 (0.75)	18.51 (0.80)	--	8.04 (0.18)	0.93 (0.10)	0.15 (0.02)	(1.20) (0.32)
PolyThieno-Naph	76.49 (0.51)	13.45 (0.91)	--	7.21 (0.79)	0.83 (0.10)	0.15 (0.03)	0.94 (0.47)
PolyThieno-Fluo	75.44 (2.32)	12.85 (0.35)		7.62 (1.00)	0.83 (0.34)	0.11 (0.08)	2.58 (1.46)
PolyThieno-Pyr	80.81 (0.41)	10.78 (0.07)	--	6.49 (0.65)	0.74 (0.24)	0.14 (0.01)	1.04 (0.29)

1

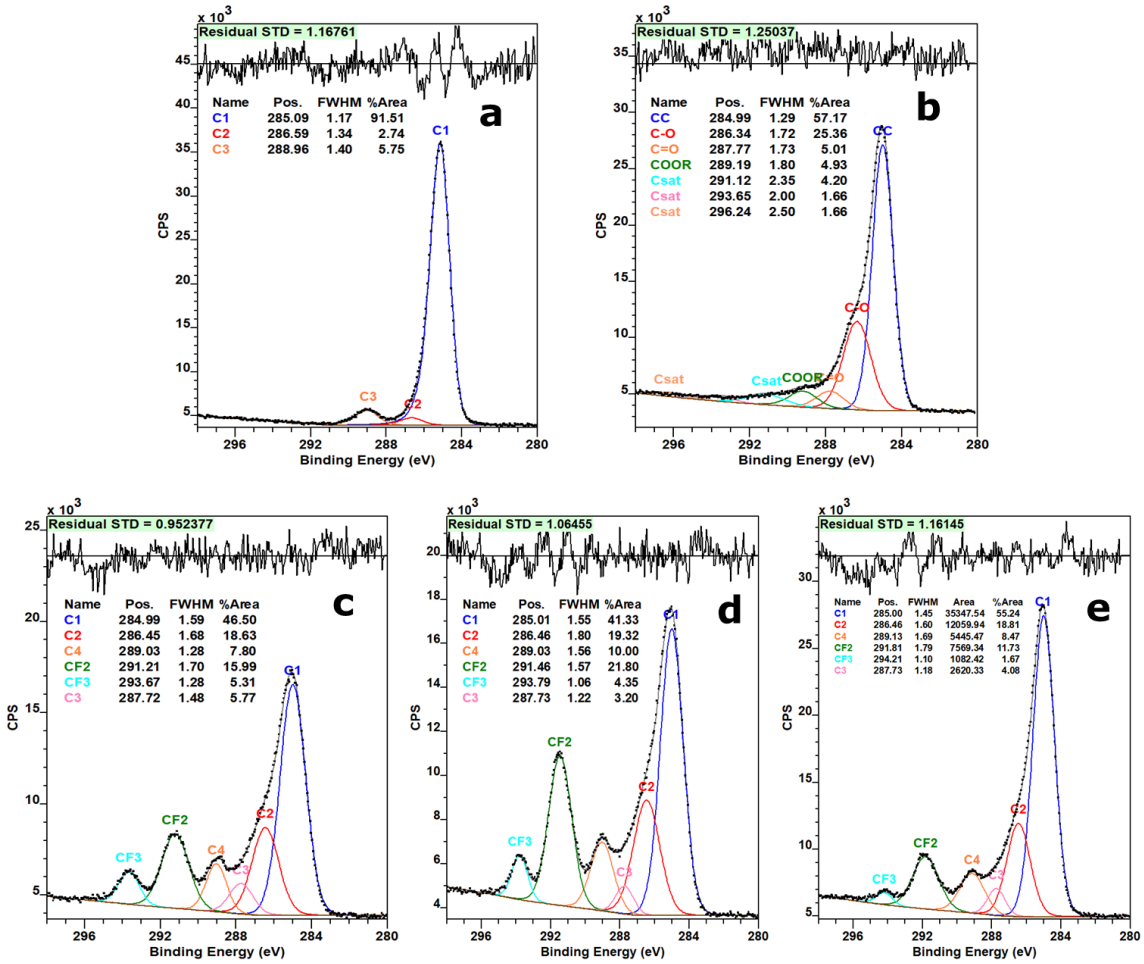

Figure 4. C 1s core level spectra of the ITO substrate (a), after PolyThieno-OH (b), after Poly-Thieno-F_n grafting: C_4F_9 (c), C_6F_{13}(d) and C_8F_{17} (e). (note: intensity in Counts per Second, CPS).

Table 4. Theoretical compositions of the compounds used in this study (excluding H) and normalized aromatic content.

	Composition (at%)					
Sample	C	O	S	F	Formula (excluding H)	Normalized aromatic content
PolyThieno-OH	70.0	10.0	20.0	--	C_7S_2O	--

PolyThieno-F_4	51.8	7.4	7.4	33.3	$C_{14}O_2S_2F_9$	--
PolyThieno-F_6	48.5	6	6	39.4	$C_{16}O_2S_2F_{13}$	--
PolyThieno-F_8	46.1	5.1	5.1	43.6	$C_{18}O_2S_2F_{17}$	--
PolyThieno-Ph	77.8	11.1	11.1	--	$C_{14}O_2S_2$	0.28
PolyThieno-diPh	84	8.0	8.0	--	$C_{21}O_2S_2$	0.35
PolyThieno-Naph	81.8	9.1	9.1	--	$C_{18}O_2S_2$	0.33
PolyThieno-BiPh	83.3	8.3	8,3	-	$C_{20}O_2S_2$	0.33
PolyThieno-Pyr	85.7	7.1	7.1	--	$C_{24}O_2S_2$	0.40
PolyThieno-Fluor	84	8.0	8.0	--	$C_{21}O_2S_2$	0.25

Further information can be inferred from the AR-XPS data. Figure 5 (a) illustrates the In/C signal ratio of the ITO substrate as a function of the Take off Angle (ToA). As can be seen the In/C ratio drops almost linearly when decreasing the analysis depth. This indicates the presence of a relatively large carbon overlayer, the presence of which is confirmed by the estimation of the overlayer thickness using the so-called “Thickogram” method and using the Inelastic Mean Free Path (IMFP) from the Seah formula [59,60]. In fact, an hydrocarbon layer of about 1.4 nm in thickness is present on the as received ITO substrate (Figure 6). After the reaction with the Poly-Thieno-OH the estimated thickness is 0.97 nm not far from the theoretical thickness of 0.6 nm calculated on the base of geometrical bond considerations and assuming a dense packed monolayer.

Figure 5 (b) shows the F/In signal evolution as a function of the ToA for the three Poly-Thieno-F_n samples. As can be seen, the signal is almost constant until the 70 ° ToA. This indicates that the Poly-Thieno-F_n are almost parallel to the ITO substrate, supporting the idea that the grafted molecules are not straight packed respect to the ITO surface, but more likely randomly distributed onto the nanotubular structures.

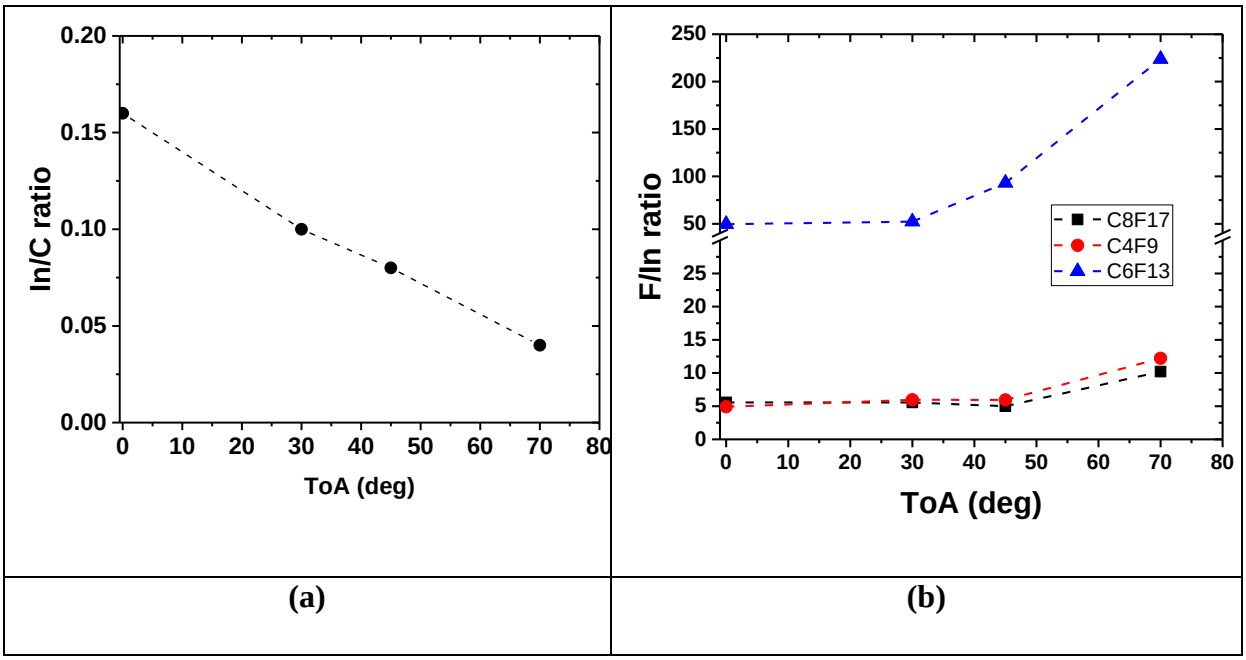

Figure 5. (a) In/C signal ratio as a function of ToA in ITO sample; (b) F/In signal ratios of the Poly-Thieno-F_n samples.

Although the theoretical thicknesses were estimated by simple geometrical considerations and that all samples show a hydrocarbon contamination the results are supporting the conclusions obtained by considering the surface compositions (Table 2) and ARXPS data presented in Figure 5.

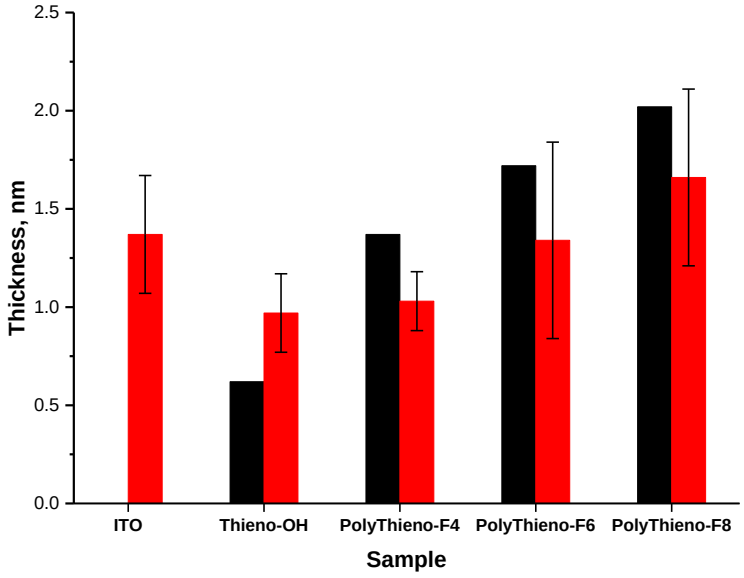

Figure 6. Theoretical (black film thicknesses from XPS data.

Apart the Thieno-OH, all the measured overlayer thicknesses are lower than the theoretical ones (Figure 6). This together with the presence of the hydrocarbon contamination layer as

discussed above, indicates that PolyThieno-F_n are not forming a vertical close packed structure on the substrate, but most likely a structure where the PolyThieno-F_n form a low angle with the ITO substrate. However, it should be also noticed that, given the nanostructured nature and large roughness of the substrate, the thicknesses of the PolyThieno-F_n can vary largely within the sample, making the overlayer estimation not very precise.

Interestingly, there is no correlation between the contact angle (Table 1) and degree of chemical functionalization of the PolyThieno-F_n surfaces. In fact, the larger content of CF_n is observed in the PolyThieno-F_6, the PolyThieno-F_8 shows the higher water CA. this result indicates that the roughness effects is predominant in determine the surface response.

ToF-SIMS analyses of ITO, Thieno-OH and the PolyThieno-F_n were also performed. Eight negative spectra were acquired for each specimen and processed using the simsMVA software and Five NMF EMs (endmembers) were obtained. Figure 7 (a) reports the NMF scores for the first three EMs showing successful grouping of samples belonging to the same specimen, whilst Figure 7 (b) illustrates the NMF scoring for the EMs 3 and 4. Samples from fluorinated SAMs, C_4F_9, C_6F_{13} and C_8F_{17}, scored high in EM 1, 2 and 3 respectively. The loadings of all EMs obtained by the NMF analysis are shown in Figure S44. The loadings provide information about which peaks are responsible for the score of the samples in the NMF space. Peaks comprised in the loadings for a certain EM are correlated with samples scoring high for the same EM. EMs 1, 2 and 3 contained characteristic peaks of the PolyThieno-F_n. All of them shared similar low mass peaks (up to 150 u) which is not surprising according to the similar constitutional structure of the SAMs, C_nF_{2n+1}. The main differences were found at higher mass where the peaks are more characteristic. Main fragments for EM 1 (C_4F_9), 2 (C_6F_{13}) and 3 (C_8F_{17}) were $C_3F_6OH^-$ (m/z =166.99), $C_5F_{10}OH^-$ (m/z =266.99) and $C_7F_{14}OH^-$ (m/z =366.99) respectively. Interestingly, the difference among these peaks is exactly ± C_2F_4 which is the difference in carbon and fluorine atoms among the PolyThieno-F_n supporting the peak assignments. EM 4 and 5 were related to Thieno-OH and ITO respectively, with loadings containing high intensity peaks for fragments containing sulfur for EM 4 and fragments containing In, Sn as well as $C_xH_yO_z$ (contaminants) for EM 5. These results confirm the successful attachment of the three different SAMs components to the Thieno-OH surface.

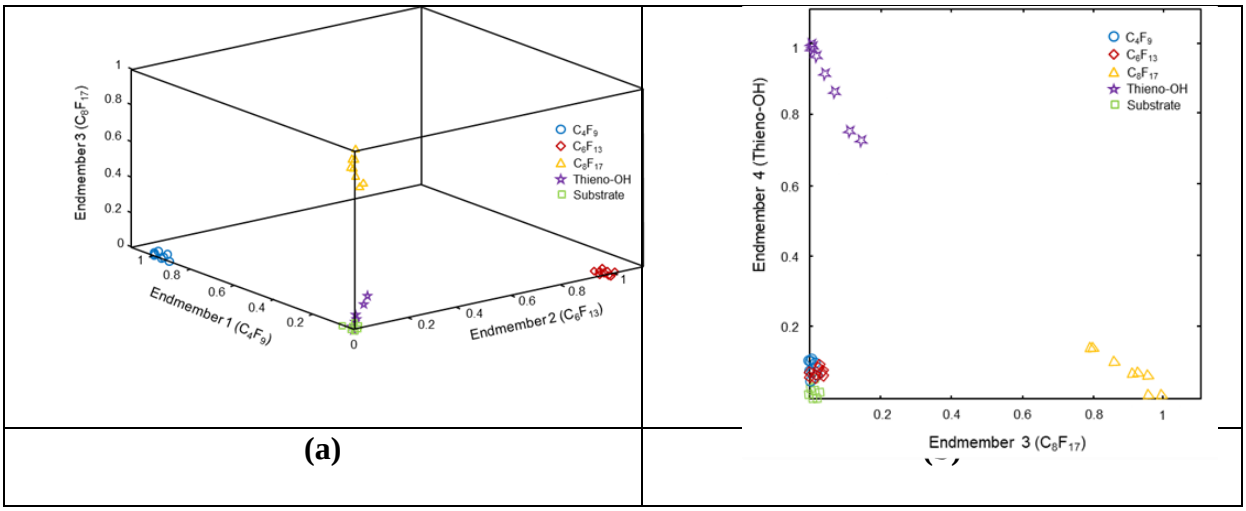

Figure 7. NMF scores of (a) EM1, 2, 3 and (b) EM 3, 4.

It is interesting to note that data from specimens PolyThieno-F_8 and Thieno-OH showed to be more dispersed toward a particular direction. This dispersion can be observed clearly by plotting EM 4 against EM 3 as reported in Figure 7 (b). Data from the PolyThieno-F_8 are dispersed towards Thieno-OH samples indicating a small but significant contribution of EM 4 characteristic peaks in the specimen surface. This might be due to a low surface grafting yield, which would explain the results obtained by XPS where it was found that PolyThieno-F_8 was the component with lower atomic concentration of fluorine, and the results regarding the surface energy, where the lowest γ_{SV} was surprisingly obtained with PolyThieno-F_6 instead of PolyThieno-F_8. In fact, looking at the loadings of EM 1, 2 and 3, it is evident that the fragments containing sulfur, which are related to the Thieno-OH, are more intense in EM 3 supporting the hypothesis of a low grafting yield for the PolyThieno-F_8.

XPS analysis of the different aromatic molecules grafted onto the ITO-PolyThieno-OH surfaces reveal a relative high level of functionalization as can be seen from the decrease of the In 3d, Sn 3d and S 2p intensities illustrated in Table 3 and the correspondent increase of the Carbon signal. However, it should be noticed that in all samples a relatively large amount surface contaminants such as Si, Na, Cl and Ca is also detected. This surface contamination can be partially explained both with sample preparation (Cl and Na) and also with sample handling (Si), whilst the presence of Ca was also observed on the starting ITO surface.

The C 1s core level spectra recorded after functionalization show very similar features in all samples as illustrated in Figure 8 for the case of Poly-Thieno-diPh. As can be seen beside the aliphatic hydrocarbon component (C1-AL ~ 285 eV), the aromatic component (C1-AR) at about 284.5 eV is also observed supporting the quantitative analysis [61,62]. Furthermore, components related to C-OH (C3 at about 286.5), COO(H) (C4 ~ 289.2 eV) are clearly

detected. Finally, components at higher binding energies (291-195 eV) attributable to aromatic satellites are also detected Figure 8 and Figure S5). ARXPS data provided further support to the successful functionalization; in fact the C 1s spectrum recorded at 70 ° ToA reveals an increase of the aromatic component (C1-AR in Figure 8c). This is expected in case of successful functionalization because of the higher surface sensitivity at glancing detection angles. The O 1s core level spectrum is presented in Figure 8 (b) and can be fitted with three components related to In_2O_3 (O1 ~ 530.5 eV), a second one attributable to O-C=O moieties (O2 ~ 531.8 eV) and a third one related to C-O bonds and $In(OH)_3$ (O3 ~ 533.3 eV). Comparing this result with that of Figure S 2 (bare ITO) it can be noticed a strong decrease of component O1, as expected and a corresponding increase of the component O2 due to the post grafting process. These data are in agreement with the quantitative results further vouching the success of the surface functionalization process.

Similar type of core level spectra are also observed in the case of the other aromatic molecules (Figure S 5). However, based on the analysis of the quantitative data and the C 1s core level fittings a sort of qualitative ranking related to the level of functionalization can be attempted. In particular, by normalizing the aromatic component intensity to the theoretical carbon content (Table 4), the best functionalization is obtained with Poly-Thieno-Pyr followed by Poly-Thieno-Diph, whilst Poly-Thieno-Phen is the less effective. Finally, the same level of functionalization is achieved when using Poly-Thieno-Naph and Poly-Thieno-Biph molecules.

As in the case of CF_n functionalization, no specific link between the functionalization level and the wettability properties reported in Table 1 were observed. In fact, while lower contact angles (less than 70 °) are measured in samples with low aromatic content (< 0.30), increasing the functionalization level did not result in a systematic increase of the water contact angle. This indicates that, beside the functionalization level, (nano)structural character of the surface is playing a paramount role in defining the wettability properties of these surfaces making difficult the evaluation of the surface chemistry contribute.

The S 2p core level spectra (Figure S6 in supporting information) are similar to those observed in the samples functionalized with PolyThione-F_n molecules and consist of two doublets related to C-S moieties and some oxidized sulfur likely related to the Thieno-OH degradation during sample preparation and aging.

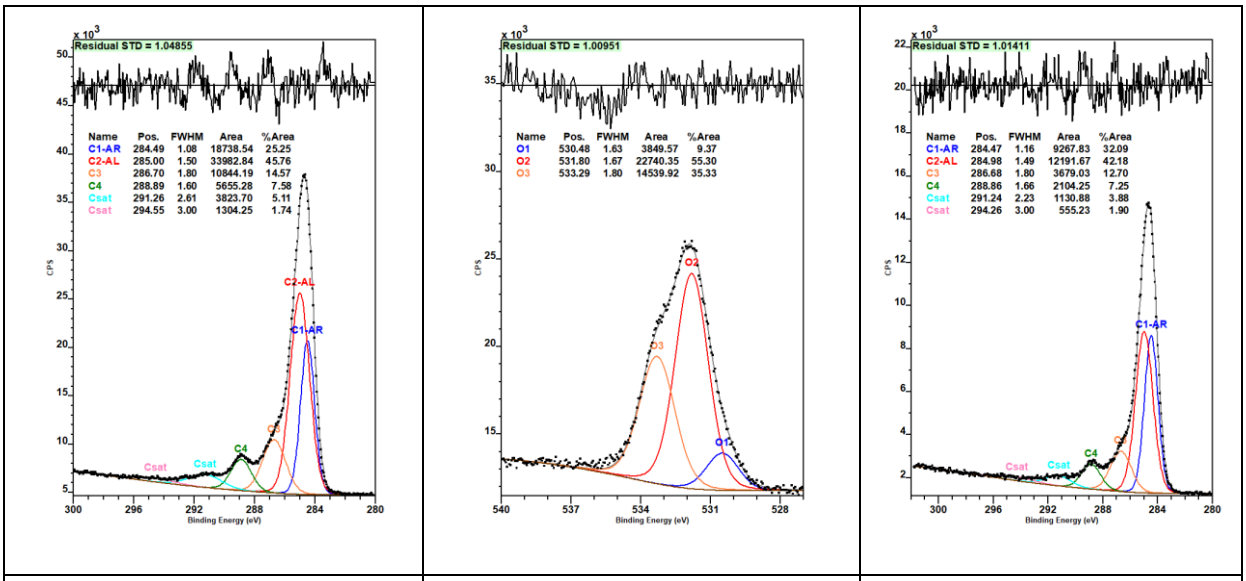

(a) **(b)** **(c)**

Figure 8. Photoelectron core level spectra of the PolyThieno-diPh: C 1s and O 1s recorded at 0 ° ToA, (a), (b) at 70 ° ToA (c).

3.4. Fluorescence of surfaces

For the fluorescence properties of surfaces, it was not possible to measure absorption and emission spectra on any ITO films with a standard steady-state equipment due to high absorption (dark grey to black colour) and diffusion of any surface. More precisely, it was not possible to measure any quantum efficiency and the spectra were already terribly difficult to record. This is probably due to the fact that starting polymer (PolyThieno-OH) being already fluorescent, the polydispersity in size of this polymer made the fluorescence analyses difficult, as already observed in electropolymerized polyfluorenes, for example [63]. Nevertheless, we were able to perform fluorescence microscopy imaging in order to compare topography and luminescence signal. PolyThieno-OH and any PolyThieno-postgrafted films are nicely luminescent (Figure 9 and ESI). Different substructures can be observed. The fluorescence images correlate well with the SEM images: showing bright rings corresponding well to the tops of the tubular shapes. The 3D-reconstruction (z-scan on Figure 8b) clearly shows a similar thickness of films (less than 5 micrometres) but with different surface coverage. Using similar illumination, it seems that PolyThieno-postgrafted films with polyaromatics are brighter than parent PolyThieno-OH (ESI), this might come from the intrinsic chromophore luminescence.

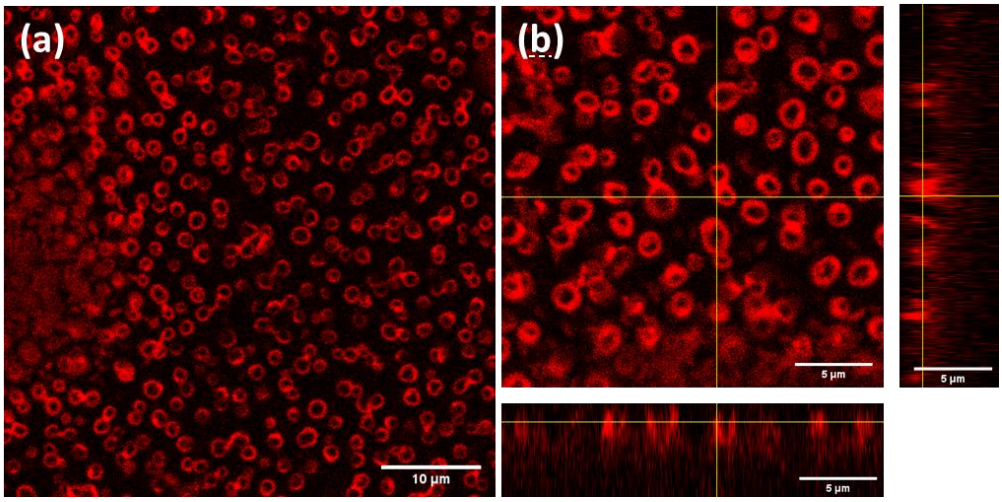

Figure 9. Fluorescence imaging and orthogonal view of PolyThieno-BiPh, (λex: 488nm λem: 510-650nm). The surrounding medium is distilled water.

4. Conclusions

Here, we tried to investigate or confirm [11] how surface nanotructures with nanotubular shape give exceptional properties. We studied not only the adhesive but also the fluorescence properties of conducting polymer nanotubes made by soft template electropolymerization and *post*-grafting. Different substituents were studied such a fluorinated chains and aromatic groups, in order to tune these surface properties. For example, XPS and ToF-SIMS analyses demonstrated that using fluorinated chains of various length (C_4F_9, C_6F_{13} and C_8F_{17}), the surface hydrophobicity and oleophobicity did not increase with the fluorinated chain length because the *post*-grafting yields are not the same and also because of the presence of nanoroughness after *post*-grafting. These surfaces also displayed strong water adhesion known as the petal effect [42] and responsible of the gecko's foot adhesion [8]. They were also nicely fluorescent before and after *post*-grafting. We would like to underline that the main goal of this paper was to understand the role of the chemical functionalization of nanostrucrured surfaces on their wetting properties. However, we believe this work could find many practical applications, in the future, such as in liquid transport for water and oil harvesting systems [65,66], as well as in stimuli responsive antibacterial surfaces [67].

5. Acknowledgement

Part of experimental data used in this research were generated through access to the Nanobiotechnology Laboratory under the Framework of access to the Joint Research Centre Physical Research Infrastructures of the European Commission (Project PostGraf). We thank the Centre de Photonique pour la Biologie et les Matériaux (CPBM) of the Centre Laser de l'Université Paris-Sud (CLUPS/LUMAT FR2764, Orsay, France) for allowing us to use the confocal microscope facility. RMR thanks Région Ile-de-France and DIM Nano-K, LUMAT and LabEx Charmmmat for their support. The group thanks the Centre Commun de Microscopie Appliquée (CCMA, Université Côte d'Azur) for the preparation of the substrates necessary for the SEM analyses. This work was supported by CNRS GDR 2088 « BIOMIM ».

6. Author contributions

Ananya Sathanikan did post-grafting and surface wetting properties, Giacomo Ceccone and Jorge Bañuls-Ciscar did the XPS and Tof-SIMS analyses, Miaobo Pan and Rachel Méallet-Renault did the fluorescence analyses, Fadwa Kamal, Talia Bsaibess, Anne Gaucher and Damien Prim did the chemical syntheses, Thierry Darmanin did the electropolymerization and SEM images, Pascal Colpo, Sonia Amigoni and Frédéric Guittard worked on the discussion part.

References

[1] M. Yang, N.A. Kotov, Nanoscale helices from inorganic materials, J. Mater. Chem. 21 (2011) 6775–6792.

[2] P. Wang, M.E. Nasir, A.V. Krasavin, W. Dickson, Y. Jiang, A.V. Zayats, Plasmonic metamaterials for nanochemistry and sensing, Acc. Chem. Res. 52 (2019) 3018–3028.

[3] X. Zhang, A. Wang, X. Liu, J. Luo, Dendrites in lithium metal anodes: Suppression, regulation, and elimination, Acc. Chem. Res. 52 (2019) 3223–3232.

[4] B. Su, Y. Tian, L. Jiang, Bioinspired interfaces with superwettability: From materials to chemistry, J. Am. Chem. Soc. 138 (2016) 1727–1748.

[5] J. Mei, T. Liao, L. Kou, Z. Sun, Two-dimensional metal oxide nanomaterials for next-generation rechargeable batteries, Adv. Mater. 29 (2017) 1700176.

[6] A. Marmur, Hydro- hygro- oleo- omni-phobic? Terminology of wettability classification, Soft Matter 8 (2012) 6867–6870.

[7] T. Darmanin, F. Guittard, Superhydrophobic and superoleophobic properties in nature, Mater. Today 18 (2015) 273–285.
[8] Y. Zhang, S. Ma, B. Li, B. Yu, H. Lee, M. Cai, S.N. Gorb, F. Zhou, W. Liu, Gecko's feet-inspired self-peeling switchable dry/wet adhesive, Chem. Mater. 33 (2021) 2785–2795.
[9] L. Qu, L. Dai, M. Stone, Z. Xia, Z. L. Wang, Carbon nanotube arrays with strong shear binding-on and easy normal lifting-off, Science 322 (2008) 238–242.
[10] L. Ge, S. Sethi, L. Ci, P. M. Ajayan, A. Dhinojwala, Carbon nanotube-based synthetic gecko tapes, Proc. Natl. Acad. Sci. U.S.A. 104 (2007) 10792–10795.
[11] Z. Cheng, J. Gao, L. Jiang, Tip geometry controls adhesive states of superhydrophobic surfaces, Langmuir 26 (2010) 8233–8238.
[12] K.K.S. Lau, J. Bico, K.B.K. Teo, M. Chhowalla, G.A.J. Amaratunga, W.I. Milne, G.H. McKinley, K.K. Gleason, Superhydrophobic carbon nanotube forests, Nano Lett. 3 (2003) 1701–1705.
[13] Y. Lai, F. Pan, C. Xu, H. Fuchs, L. Chi, In situ surface-modification-induced superhydrophobic patterns with reversible wettability and adhesion, Adv. Mater. 25 (2013) 1682–1686.
[14] H. Fan, Z. Guo, Robust multi-functional slippery surface with hollow ZnO nanotube structures, New J. Chem. 44 (2020) 15483–15491.
[15] H.-A. Lin, S.-C. Luo, B. Zhu, C. Chen, Y. Yamashita, H.-h. Yu, Molecular or nanoscale structures? The deciding factor of surface properties on functionalized poly(3,4-ethylenedioxythiophene) nanorod arrays, Adv. Funct. Mater. 23 (2013) 3212–3219.
[16] L. Lee, S.J. Park, Porous anodic aluminum oxide: Anodization and templated synthesis of functional nanostructures, Chem. Rev. 114 (2014) 7487–7556.
[17] N. Subramanian, A. Qamar, A. Alsaadi, A. Gallo Jr., M.G. Ridwan, J.G. Lee, S. Pillai, S. Arunachalam, D. Anjum, F. Sharipov, N. Ghaffour, H. Mishra, Evaluating the potential of superhydrophobic nanoporous alumina membranes for direct contact membrane distillation, J. Colloid Interface Sci. 533 (2019) 723–732.
[18] C. Debiemme-Chouvy, Template-free one-step electrochemical formation of polypyrrole nanowire array, Electrochem. Commun. 11 (2009) 298–301.
[19] A. Fakhry, H. Cachet, C. Debiemme-Chouvy, Mechanism of formation of templateless electrogenerated polypyrrole nanostructures, Electrochim. Acta 179 (2015) 297–303.
[20] L. Qu, G. Shi, F. Chen, J. Zhang, Electrochemical growth of polypyrrole microcontainers, Macromolecules 36 (2003) 1063−1067.

[21] B. Parakhonskiy, D. Shchukin, Polypyrrole microcontainers: Electrochemical synthesis and characterization, Langmuir 31 (2015) 9214−9218.

[22] S. Gupta, Hydrogen bubble-assisted syntheses of polypyrrole micro/nanostructures using electrochemistry: Structural and physical property characterization, J. Raman Spectrosc. 39 (2008) 1343–1355.

[23] J.T. Kim, S.K. Seol, J.H. Je, Y. Hwu, G. Margaritondo, The microcontainer shape in electropolymerization on bubbles, Appl. Phys. Lett. 94 (2009) 034103.

[24] T. Darmanin, E.L. Klimareva, I. Schewtschenko, F. Guittard, I.F. Perepichka, Exceptionally strong effect of small structural variations in functionalized 3,4-phenylenedioxythiophenes on the surface nanostructure and parahydrophobic properties of their electropolymerized films, Macromolecules 52 (2019) 8088–8102.

[25] T. Darmanin, F. Guittard, A one-step electrodeposition of homogeneous and vertically aligned nanotubes with parahydrophobic properties (high water adhesion), J. Mater. Chem. A 4 (2016) 3197–3203.

[26] O. Sane, A. Diouf, G. Morán Cruz, F. Savina, R. Méallet-Renault, S. Amigoni, S.Y. Dieng, F. Guittard, T. Darmanin, Coral-like nanostructures, Mater. Today 31 (2019) 119–120.

[27] T. Darmanin, R. Bombera, P. Colpo, A. Valsesia, J.-P. Laugier, F. Rossi, F. Guittard, Bioinspired rose-petal-like substrates generated by electropolymerization on micropatterned gold substrates, ChemPlusChem 82 (2017) 352–357.

[28] C. Fradin, F. Orange, S. Amigoni, C.R. Szczepanski, F. Guittard, T. Darmanin, Micellar formation by soft template electropolymerization in organic solvents, J. Colloid Interface Sci. 590 (2021) 260–267.

[29] O. Sane, A. Diouf, M. Pan, G. Morán Cruz, F. Savina, R. Méallet-Renault, S.Y. Dieng, S. Amigoni, F. Guittard, T. Darmanin, Nanotubular structures through templateless electropolymerization using thieno[3,4-b]thiophene derivatives with different substituents and water content, Electrochim. Acta 320 (2019) 134594.

[30] E. El Kout, R. Ben Trad, M. El Kateb, M. Beji, J.-P. Laugier, J.-P.; Godeau, F. Guittard, F.; Darmanin, T.; Combining Staudinger reductive amination and amidification for the control of surface hydrophobicity and water adhesion by introducing heterobifunctional groups: Post- and ante- approach, Macromol. Chem. Phys. 218 (2017) 1700250.

[31] L. Ma, S. Jayachandran, Z. Li, Z. Song, W. Wang, X. Luo, Antifouling and conducting PEDOT derivative grafted with polyglycerol for highly sensitive electrochemical protein detection in complex biological media. J. Electroanal. Chem. 840 (2019) 272–278.

[32] E. Pierce, F.J. Carmona, A. Amirfazli, Understanding of sliding and contact angle results in tilted plate experiments, Colloids Surf., A 323 (2008) 73–82.

[33] S. Tougaard, Accuracy of the non-destructive surface nanostructure quantification technique based on analysis of the XPS or AES peak shape, Surf. Interface Anal. 26 (1998) 249–269.

[34] S. Tougaard, F. Yubero, QUEELS software package for calculation of surface effects in electron spectra, Surf. Interface Anal. 36 (2004) 824–827.

[35] A. Henderson, Multivariate analysis of SIMS spectra, in: J.C. Vickerman, D. Briggs (Eds.), TOF- SIMS Mater. Anal. by mass spectrom., Surface Spectra (UK), 2013, p. 449.

[36] B.J. Tyler, G. Rayal, D.G. Castner, Multivariate analysis strategies for processing ToF-SIMS images of biomaterials, Biomaterials 28 (2007) 2412–2423.

[37] D.J. Graham, D.G. Castner, Multivariate analysis of ToF-SIMS data from multicomponent systems: The why, when, and how, Biointerphases 7 (2012) 1–12.

[38] G.F. Trindade, M.L. Abel, J.F. Watts, Non-negative matrix factorisation of large mass spectrometry datasets, Chemom. Intell. Lab. Syst. 163 (2017) 76–85.

[39] G.F. Trindade, M.L. Abel, J.F. Watts, simsMVA: A tool for multivariate analysis of ToF-SIMS datasets, Chemom. Intell. Lab. Syst. 182 (2018) 180–187.

[40] J. Shlens, A tutorial on principal component analysis, 2014, arXiv preprint arXiv, 1404.1100.

[41] H.B. Eral, D.J.C.M. ’t Mannetje, J.M. Oh, Contact angle hysteresis: A review of fundamentals and applications, Colloid Polym. Sci. 291 (2013) 247–260.

[42] B. Krasovitski, A. Marmur, Drops down the hill: Theoretical study of limiting contact angles and the hysteresis range on a tilted plate, Langmuir 21 (2005) 3881–3885.

[43] B. Krasovitski, A. Marmur, Line tension on curved surfaces: Liquid drops on solid micro- and nanospheres, Langmuir 18 (2002) 8919–8923.

[44] L. Feng, Y. Zhang, J. Xi, Y. Zhu, N. Wang, F. Xia, L. Jiang, Petal effect: A superhydrophobic state with high adhesive forc, Langmuir 24 (2008) 4114–4119.

[45] B. Bhushan, M. Nosonovsky, The rose petal effect and the modes of superhydrophobicity, Phil. Trans. R. Soc. A. 368 (2010) 4713–4728.

[46] C.R. Szczepanski, T. Darmanin, F. Guittard, Recent advances in the study and design of parahydrophobic surfaces: From natural examples to synthetic approaches, Adv. Colloid Interface Sci. 241 (2017) 37–61.

[47] Z. Guo, L. Zhang, D. Monga, H.A. Stone, X. Dai, Hydrophilic slippery surface enabled coarsening effect for rapid water harvesting, Cell Rep. Phys. Sci. 2 (2021) 100387.

[48] R.N. Wenzel, Resistance of solid surfaces to wetting by water, Ind. Eng. Chem. 28 (1936) 988–994.

[49] A.B.D. Cassie, S. Baxter, Wettability of porous surfaces, Trans. Faraday Soc. 40 (1944) 546–551.

[50] T. Young, An essay on the cohesion of fluids, Philos. Trans. R. Soc. London 95 (1805) 65.

[51] D.K. Owens, R.C. Wendt, Estimation of the surface free energy of polymers, J. Appl. Poly. Sci. 13 (1969) 1741–1747.

[52] C. Donley, D. Dunphy, D. Paine, C. Carter, K. Nebesny, P. Lee, D. Alloway, N.R. Armstrong, Characterization of Indium−Tin oxide interfaces using X-ray photoelectron spectroscopy and redox processes of a chemisorbed probe molecule: Effect of surface pretreatment conditions, Langmuir 18 (2002) 450−457.

[53] G.G. Khan, S. Ghosh, A. Sarkar, G. Mandal, G.D. Mukherjee, U. Manju, N. Banu, B.N. Dev, Defect engineered d0 ferromagnetism in tin-doped indium oxide nanostructures and nanocrystalline thin-films, J. Appl. Phys. 118 (2015) 074303.

[54] T. Dang, J. Lefebvre, J.D. Wuest, Recycling Indium Tin oxide (ITO) electrodes used in thin-film devices with adjacent hole-transport layers of metal oxides, ACS Sustainable Chem. Eng. 3 (2015) 3373−3381.

[55] H. Yue, L. Kong, X. Li, Y. Zhang, H. Du, Y. Dong, J. Zhao, J. Zhang, Soluble neutral green-colored polymers based on propylenedioxythiophene, benzene and thieno[3,4-b]pyrazine, and their electrochromic properties, Synth. Met. 261 (2020) 116320.

[56] J. Kettle, Z. Ding, M. Horie, G.C. Smith, XPS analysis of the chemical degradation of PTB7 polymers for organic photovoltaics, Org. Electron. 39 (2016) 222–228.

[57] G. Beamson, D. Briggs (eds), “ESCA database of polymers”, Surface Spectra, UK, 2000.

[58] R. La Spina, Influence of different cleaning processes on the surface chemistry of gold nanoparticles, Biointerphases 12 (2017) 031003.

[59] S. Ray, A.G. Shard, Quantitative analysis of adsorbed proteins by X-ray photoelectron spectroscopy, Anal. Chem. 83 (2011) 8659–8666.

[60] P.J. Cumpson, The thickogram: A method for easy film thickness measurement in XPS, Surf. Interface Anal. 29 (2000) 403–406.

[61] M.P. Seah, W.A. Dench, Quantitative electron spectroscopy of surfaces: A standard data base for electron inelastic mean free paths in solids, Surf. Interface Anal. 1 (1979) 2–11.

[62] T.R. Gengenbach, G.H. Major, M.R. Linford, C.D. Easton, Practical guides for X-Ray photoelectron spectroscopy (XPS): Interpreting the carbon 1s spectrum, J. Vac. Sci. Technol. A 39 (2021) 013204.

[63] D. Briggs, Surface analyis of polymers by XPS and static SIMS, (eds. D.R. Clarke, S. Suresh, I.M. Ward), CambridgeUniv Press, 1998.

[64] G. Ramos Chagas, X. Xie, T. Darmanin, K. Steenkeste, A. Gaucher, D. Prim, R. Méallet-Renault, G. Godeau, S. Amigoni, F. Guittard, Electrodeposition of polypyrenes with tunable hydrophobicity, water adhesion and fluorescence properties, J. Phys. Chem. C 120 (2016) 7077–7087.

[65] S. Ozden, L. Ge, T.N. Narayanan, A.H.C. Hart, H. Yang, S. Sridhar, R. Vajtai, P.M. Ajayan, Anisotropically functionalized carbon nanotube array based hygroscopic scaffolds, ACS Appl. Mater. Interfaces 6 (2014) 10608–10613.

[66] Y. Hou, Y. Shang, M. Yu, C. Feng, H. Yu, S. Yao, Tunable water harvesting surfaces consisting of biphilic nanoscale topography, ACS Nano 12 (2018) 11022–11030.

[67] T.A. Khattab, M. E. El-Naggar, M.S. Abdelrahman, A. Aldalbahi, M.R. Hatshan, Facile development of photochromic cellulose acetate transparent nanocomposite film immobilized with lanthanidedoped pigment: ultraviolet blocking, superhydrophobic, and antimicrobial activity, Luminescence 36 (2021) 543–555.

Figures captions

Scheme 1. Strategy used to form conducting polymer nanotubes with various substituents.

Figure 1. SEM images of the polymer surfaces electrodeposited from the monomer Thieno-OH (10 mM) in 0.1 M Bu_4NClO_4 / CH_2Cl_2 + H_2O in potentiodynamic conditions by cyclic voltammetry (E = –1 / +1.77 V) after 1 scan. The pictures are taken without (up) and with a substrate inclination of 45 ° (down).

Figure 2. Representative SEM images of the polymer surfaces after *post*-treatment with fluorenone (PolyThieno-Fluorenone). The pictures are taken without (up) and with a substrate inclination of 45 ° (down).

Figure 3. Picture of a water droplet on the polymer surfaces after *post*-treatment with F_6 (PolyThieno-F_6) with a substrate inclination of 90°.

Figure 4. C 1s core level spectra of the ITO substrate (a), after PolyThieno-OH (b), after Poly-Thieno-F_n grafting: C_4F_9 (c), C_6F_{13}(d) and C_8F_{17} (e). (note: intensity in Counts per Second, CPS).

Figure 5. (a) In/C signal ratio as a function of ToA in ITO sample; (b) F/In signal ratios of the Poly-Thieno-F_n samples.

Figure 6. Theoretical (black film thicknesses from XPS data.

Figure 7. NMF scores of (a) EM1, 2, 3 and (b) EM 3, 4.

Figure 8. Photoelectron core level spectra of the PolyThieno-diPh: C 1s and O 1s recorded at 0 ° ToA, (a), (b) at 70 ° ToA (c).

Figure 9. Fluorescence imaging and orthogonal view of PolyThieno-BiPh, (λex: 488nm λem: 510-650nm). The surrounding medium is distilled water.

Table 1. Apparent contact angles (θ) with different probe liquids of different nantubular surfaces.

Polymer	θ_{water} [deg]	θ_{diiodo} [deg]	θ_{hexa} [deg]
PolyThieno-OH	92.1 ± 7.1	0	0
PolyThieno-F_4	129.0 ± 4.6	117.0 ± 5.5	30.5 ± 6.8
PolyThieno-F_6	122.7 ± 4.6	130.8 ± 0.9	83.4 ± 2.1
PolyThieno-F_8	130.5 ± 3.8	125.0 ± 4.9	90.7 ± 3.5
PolyThieno-Ph	98.6 ± 5.5	0	0
PolyThieno-diPh	115.0 ± 5.4	0	0
PolyThieno-BiPh	112.6 ± 3.5	0	0
PolyThieno-Naph	92.2 ± 5.8	0	0
PolyThieno-Fluo	98.4 ± 6.0	0	0
PolyThieno-Pyr	92.4 ± 6.4	0	0
PolyThieno-Fluorenone	112.0 ± 2.4	0	0
PolyThieno-AceTetra	85.8 ± 4.9	0	0
PolyThieno-PheTetra	79.8 ± 6.6	0	0
PolyThieno-PyrTetra	106.2 ± 2.3	0	0

Table 2. Apparent contact angles (θ) with different probe liquids as well as the surface energy of the corresponding smooth surfaces (γ_{sv}) and the dispersive (γ^D_{sv}) and polar (γ^P_{sv}) parts.

Polymer	θ^Y_{water} [deg]	θ^Y_{diiodo} [deg]	θ^Y_{hexa} [deg]	γ_{sv} [mN m^{-1}]	γ^D_{sv} [mN m^{-1}]	γ^P_{sv} [mN m^{-1}]
PolyThieno-OH	49.4 ± 3.0	36.8 ± 5.1	0	52.8	28.1	24.7
PolyThieno-F_4	95.3 ± 2.7	62.4 ± 1.5	33.1 ± 1.6	26.2	24.2	2.0
PolyThieno-F_6	101.4 ± 2.4	68.5 ± 2.1	42.8 ± 4.4	22.7	21.6	1.1
PolyThieno-F_8	100.4 ± 2.5	65.5 ± 1.5	35.7 ± 3.3	24.5	23.4	1.1
PolyThieno-Ph	61.6 ± 1.7	19.8 ± 4.8	0	47.3	32.6	14.7
PolyThieno-diPh	81.9 ± 2.8	20.5 ± 2.4	0	38.8	34.6	4.1
PolyThieno-BiPh	82.3 ± 2.6	17.8 ± 3.0	0	38.9	35.0	3.9
PolyThieno-Naph	78.2 ± 1.3	16.5 ± 2.9	0	40.2	34.7	5.5
PolyThieno-Fluo	69.5 ± 5.0	15.0 ± 3.9	0	43.7	33.9	9.8
PolyThieno-Pyr	78.5 ± 1.8	15.1 ± 5.5	0	40.3	34.9	5.4
PolyThieno-Fluorenone	90.7 ± 2.7	11.9 ± 1.9	0	38.0	36.7	1.3

PolyThieno-AceTetra	77.5 ± 0.4	12.9 ± 1.3	0	40.6	34.3	6.3
PolyThieno-PheTetra	76.9 ± 2.9	19.5 ± 5.0	0	39.8	35.0	4.8
PolyThieno-PyrTetra	79.9 ± 2.9	13.0 ± 2.6	0	40.3	36.7	1.3

1

2 **Table 3.** Surface compositions obtained from XPS survey spectra.

	Concentration (at%)						
Sample ID	C1s	O1s	F1s	S2p	In3d	Sn3d	Rest Si, Ca,N, Cl
ITO	67.57 (4.51)	20.35 (2.04)	--	--	9.65 (2.43)	1.33 (0.17)	<2
PolyThieno-OH	61.43 (2.10)	17.91 (1.60)	--	13.73 (1.76)	4.23 (1.81)	0.50 (0.28)	<1
PolyThieno-F_4	47.43 (0.73)	20.03 (1.03)	20.17 (0.99)	6.26 (0.36)	4.22 (0.69)	0.82 (0.05)	<1
PolyThieno-F_6	48.64 (1.76)	14.28 (0.71)	28.58 (1.34)	6.28 (0.29)	0.71 (0.55)	0.37 (0.06)	<1
PolyThieno-F_8	55.44 (1.69)	18.76 (1.99)	15.59 (1.59)	7.47 (1.42)	1.42 (0.47)	0.37 (0.05)	<1
PolyThieno-Ph	66.27 (1.77)	23.14 (1.42)		7.70 (1.259	1.29 (0.17)	0.17 (0.02)	0.97 (0.40)
PolyThieno-diPh	78.64 (0.65)	11.77 (0.83)	--	7.94 (0.43)	0.69 (0.22))	0.07 (0.04)	0.6 (0.42)
PolyThieno-BiPh	71.22 (0.75)	18.51 (0.80)	--	8.04 (0.18)	0.93 (0.10)	0.15 (0.02)	(1.20) (0.32)
PolyThieno-Naph	76.49 (0.51)	13.45 (0.91)	--	7.21 (0.79)	0.83 (0.10)	0.15 (0.03)	0.94 (0.47)

PolyThieno-Fluo	75.44 (2.32)	12.85 (0.35)		7.62 (1.00)	0.83 (0.34)	0.11 (0.08)	2.58 (1.46)
PolyThieno-Pyr	80.81 (0.41)	10.78 (0.07)	--	6.49 (0.65)	0.74 (0.24)	0.14 (0.01)	1.04 (0.29)

Table 4. Theoretical compositions of the compounds used in this study (excluding H) and normalized aromatic content.

	Composition (at%)					
Sample	C	O	S	F	Formula (excluding H)	Normalized aromatic content
PolyThieno-OH	70.0	10.0	20.0	--	C_7S_2O	--
PolyThieno-F_4	51.8	7.4	7.4	33.3	$C_{14}O_2S_2F_9$	--
PolyThieno-F_6	48.5	6	6	39.4	$C_{16}O_2S_2F_{13}$	--
PolyThieno-F_8	46.1	5.1	5.1	43.6	$C_{18}O_2S_2F_{17}$	--
PolyThieno-Ph	77.8	11.1	11.1	--	$C_{14}O_2S_2$	0.28
PolyThieno-diPh	84	8.0	8.0	--	$C_{21}O_2S_2$	0.35
PolyThieno-Naph	81.8	9.1	9.1	--	$C_{18}O_2S_2$	0.33
PolyThieno-BiPh	83.3	8.3	8,3	-	$C_{20}O_2S_2$	0.33
PolyThieno-Pyr	85.7	7.1	7.1	--	$C_{24}O_2S_2$	0.40
PolyThieno-Fluor	84	8.0	8.0	--	$C_{21}O_2S_2$	0.25